PWM Step-Up Converter Integrating Differential Power Processing Converter to Enhance Energy Yield of Partially-Shaded Photovoltaic Panels

Yusuke Sasaki
Department of Electrical and Electronic Engineering
Ibaraki University
Ibaraki, Japan
19nm630r@vc.ibaraki.ac.jp

Hayato Sato
Department of Electrical and Electronic Engineering
Ibaraki University
Ibaraki, Japan
18nm631a@vc.ibaraki.ac.jp

Masatoshi Uno
Department of Electrical and Electronic Engineering
Ibaraki University
Ibaraki, Japan
masatoshi.uno.ee@vc.ibaraki.ac.jp

***Abstract*— Partial shading on a photovoltaic (PV) panel consisting of multiple substrings is known to trigger a significant reduction in power yield and the occurrence of multiple maximum power points (MPPs). Although differential power processing (DPP) converters can preclude the negative influences of partial shading, an additional DPP converter is separately required in addition to an existing step-up converter for panel control, resulting in increased circuit volume and system complexity. This paper proposes a novel integrated converter that realizes system simplification and circuit miniaturization by integrating a PWM step-up converter and a DPP converter. Laboratory and field tests were performed emulating partial shading and characteristic mismatch conditions. A local MPP successfully disappeared, and the extractable maximum power increased while boosting the panel voltage, demonstrating the efficacy of the proposed integrated converter.**

Keywords*— Photovoltaic; Partial shading; Differential power processing converter; PWM step-up converter; Integrated converter

I. Introduction

Partial shading on photovoltaic (PV) panels comprising multiple PV substrings connected in series is well known to trigger not only significant power reduction but also the occurrence of multiple maximum power points (MPPs), including one global and local MPP(s), as shown in Fig. 1(a). The occurrence of multiple MPPs confuses and hinders ordinary MPP tracking (MPPT) algorithms for tracking the global MPP. These negative influences originate from the electrical characteristic mismatch of substrings.

I–V characteristics of the shaded and unshaded substrings are shown in Fig. 1(b). As all substrings share the same current, shaded substring(s) with lower output current is bypassed by parallel-connected diodes. The bypassed substring(s) no longer contribute to power generation, and hence the generated power of the panel as a whole significantly decreases. In addition, the multiple MPPs appear on a *P–V* characteristic of the partially shaded panel due to the conducting bypass diode, as shown in Fig. 1(b). Similar situations are known to happen on curved PV panels mounted on plug-in hybrid electric vehicles' (PHEV) roof due to uneven irradiance on curved surfaces. Although an MPPT control is generally performed to maximize power yield in PV systems, the panel might operate at a local MPP that is a suboptimal point producing less power than a global MPP.

Various kinds of differential power processing (DPP) converters based on bidirectional converters [1]–[5], switched capacitor converters [6]–[11], isolated bidirectional converters [12]–[15], single-input–multi-output converters [16]–[23], etc., have been proposed to eliminate the negative influences of partial shading. A conventional DPP converter using an LLC resonant voltage multiplier [16] is shown Fig. 2, as an example. The LLC resonant voltage multiplier consists of an LLC resonant inverter and a voltage multiplier (VM). Even without feedback control, this DPP converter redistributes power from the panel to shaded substrings having the lowest voltage. All substring voltages or characteristics are nearly unified, and the negative influences of partial shading are prevented.

Meanwhile, a step-up converter is generally indispensable to bridge the voltage gap between PV panels and load or grid. Since a DPP converter and a step-up converter are separately

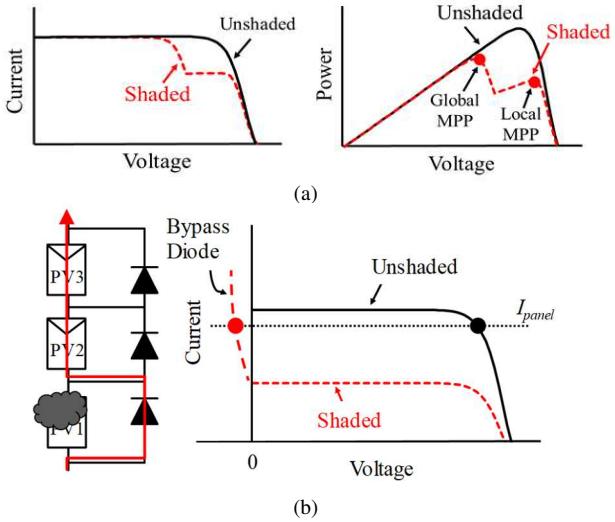

Fig. 1. PV panel under partial shading condition: (a) PV panel characteristics, (b) current flow and substring characteristics.

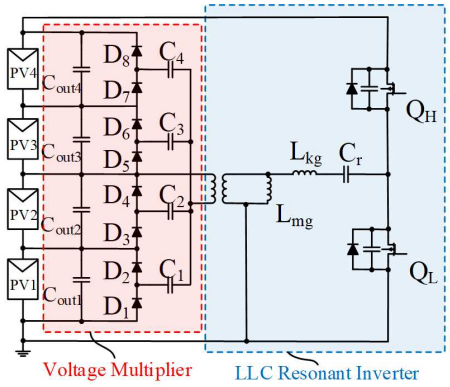

Fig. 2. Conventional DPP converter based on LLC resonant voltage multiplier [16].

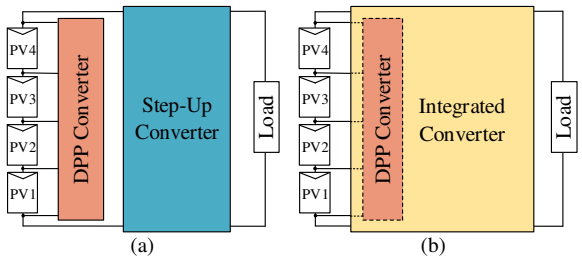

Fig. 3. Power system architectures: (a) Conventional system, (b) proposed integrated converter system.

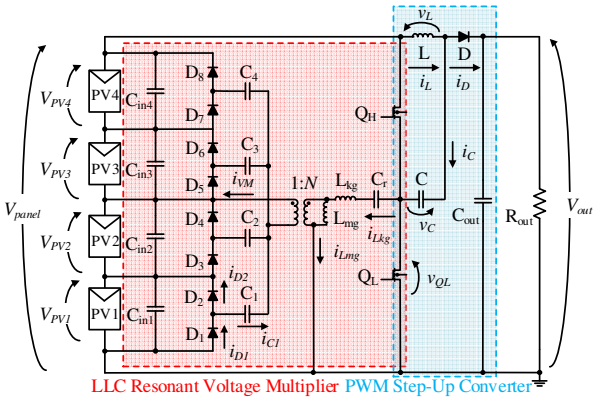

Fig. 4. Proposed PWM step-up converter integrating DPP converter.

required, conventional PV systems are prone to complexity, as shown in Fig. 3(a).

This paper proposes an integrated converter that realizes system simplification and circuit miniaturization by integrating a PWM step-up converter and a DPP converter, as shown in Fig. 3(b). The rest of this paper is organized as follows. Section II describes the proposed integrated converter. Section III presents the operation analysis, and Section IV shows the experimental results of the laboratory and field testing for four substrings connected in series under a partial shading and characteristic mismatched condition, respectively.

II. Proposed Integrated Converter

A. Derivation

The proposed integrated converter for four substrings is shown in Fig. 4. The proposed converter is derived from a combination of the conventional DPP converter based on an LLC resonant voltage multiplier [16] and the PWM step-up converter. These converters are integrated into a single unit by sharing the switches of Q_L and Q_H.

B. Features

The conventional power system using a DPP converter and traditional PWM step-up converter separately requires three switches in total; two and one switches in the DPP and step-up converters, respectively. The proposed integrated converter, on the other hand, can reduce the total switch count as low as two. In addition, the PWM step-up converter in the proposed integrated converter contributes to the miniaturization of the inductor L compared with that in a traditional PWM step-up converter because the capacitor C not only reduces the applied voltage across L but also processes a fraction of the total output power, as will be detailed in Section III.

In summary, the proposed integrated converter realizes the system simplification and circuit miniaturization by integrating two converters into a single unit while achieving the reduction of the switch count and inductor miniaturization.

The proposed converter can not only boost the panel voltage by PWM control but also automatically supply power to the shaded substrings without feedback control.

Two magnetic components (i.e., the inductor and transformer) would be integrated by properly utilizing a leakage and magnetizing inductances of a transformer, further miniaturizing the circuit. The integration of magnetic components will be a part of our future works.

III. Operation Analysis

A. Key Waveforms and Current Flow

Key operation waveforms and current flow directions when PV1 is partially shaded are shown in Figs. 5 and 6, respectively. Dead time periods are neglected, and all components in the circuit are assumed ideal. Here, the transformer winding connected to the resonant capacitor C_r is defined as the primary side, and the opposite side is defined as the secondary side.

Mode 1 [Fig. 6(a)]: Q_L and Q_H are turned on and off, respectively. The voltage of L, v_L, is $V_{panel} - V_C$. The current of L, i_L, linearly increases, and C is charged. The voltage of Q_L, v_{QL}, which corresponds to the input voltage of the resonant voltage multiplier, is zero. L_{kg} and C_r resonate, and the current of L_{kg}, i_{Lkg}, transfers to the secondary side in the form of i_{VM}. i_{VM} flows through the coupling capacitor C_1 and the high-side diode D_2. The operation shifts to the next mode when i_{Lkg} and i_{Lmg} become the same value.

Mode 2 [Fig. 6(b)]: Both i_{Lkg} and i_{Lmg} linearly decrease at the same rate, while no current flows on the secondary side. The operation of the step-up converter in this mode is identical to that in Mode 1.

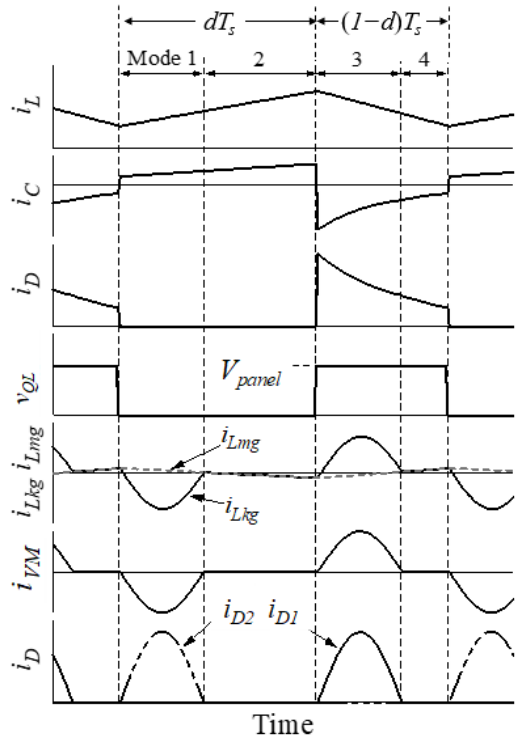

Fig. 5. Key operation waveforms.

Mode 3 [Fig. 6(c)]: Q_L and Q_H are turned off and on, respectively. v_L becomes $V_{panel} - V_{out}$, and its voltage polarity is reversed. i_L starts linearly decreases, and C is discharged. When Q_H turns on, v_{QL} becomes V_{panel}, and L_{kg} and C_r resonate again. i_{VM} on the secondary side flows through C_1 and the low-side diode D_1. The operation shifts to the next mode when i_{Lkg} and i_{Lmg} become the same value.

Mode 4 [Fig. 6(d)]: Both i_{Lkg} and i_{Lmg} linearly increase at the same rate, while no current flows on the secondary side. The operation of the step-up converter in this mode is identical to that in Mode 3. Turning on and off Q_L and Q_H, respectively brings the operation back to Mode 1.

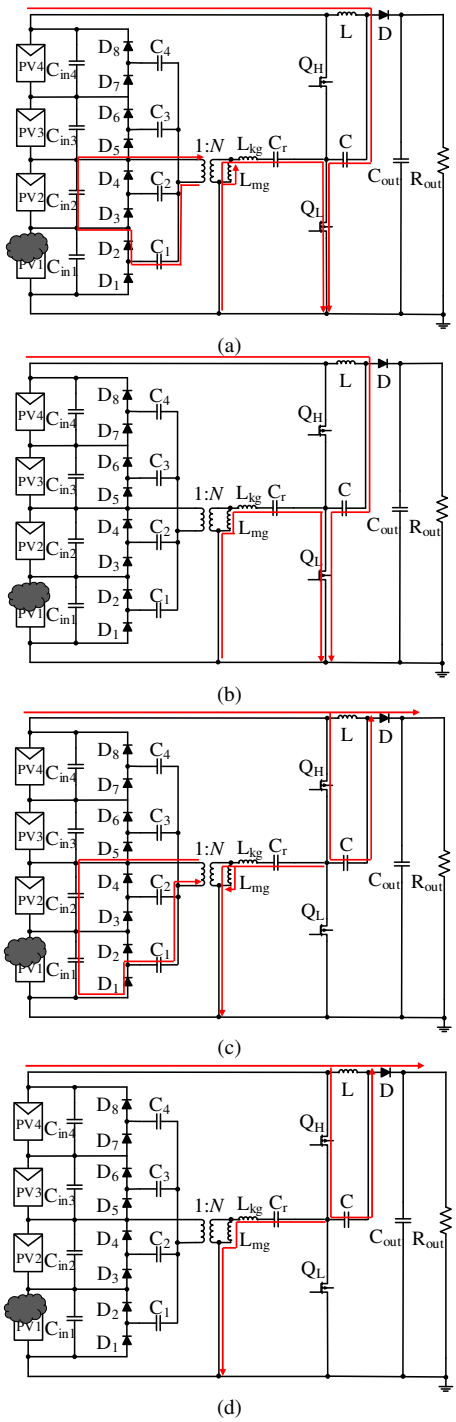

Fig. 6. Current flows paths when PV1 is shaded: (a) Mode 1, (b) Mode 2, (c) Mode 3, and (d) Mode 4.

In summary, D_1 and D_2 that are connected in parallel with the shaded substring PV1 conduct, whereas other diodes are not in operation. Since an average current of C_1 must be zero under steady-state conditions, an average current of D_1 or D_2 is identical to a current supplied to PV1 from the LLC resonant voltage multiplier. The detailed power redistribution mechanism of the LLC resonant voltage multiplier has been reported in [16].

B. PWM Step-Up Converter

The theoretical step-up voltage conversion ratio is derived from the volt-sec balance on L. Under steady-state conditions, V_C is determined by the following equation from the current paths in Modes 3 and 4 [see Figs. 6(c) and (d)];

$$V_c = V_{out} - V_{panel} \tag{1}$$

From (1), v_L is expressed as

$$v_L = \begin{cases} 2V_{panel} - V_{out} & \text{(Mode 1, 2)} \\ V_{panel} - V_{out} & \text{(Mode 3, 4)} \end{cases} \tag{2}$$

This equation suggests that L can be miniaturized as the voltage stress of L is lower than that in a traditional step-up converter. The theoretical voltage step-up conversion ratio is expressed as

$$\frac{V_{out}}{V_{panel}} = 1 + d \tag{3}$$

where d is the duty cycle or the on-period of Q_L. This equation suggests the theoretical step-up ratio is between 1.0 and 2.0.

C. LLC Resonant Voltage Multiplier

The LLC resonant inverter is powered by the panel and produces ac voltage/current, which is transferred to the secondary side of the transformer. Here, in order to supply a current to shaded substrings independently of d, half the resonant period must be shorter than the dT_s and $(1-d)T_s$, as shown in the theoretical waveform in Fig. 5, where T_s being the switching period. Therefore, the switching frequency f_s (= $1/T_s$) is expressed as

$$f_S \le \begin{cases} 2df_r = \dfrac{d}{\pi\sqrt{L_{kg}C_r}} \\ 2(1-d)f_r = \dfrac{1-d}{\pi\sqrt{L_{kg}C_r}} \end{cases} \tag{4}$$

where f_r is the resonant frequency. Thereby, f_s should be determined in consideration of a variation range of d at a given f_r.

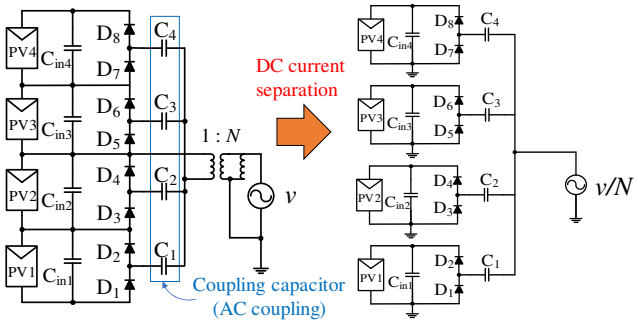

Fig. 7. Transformation of voltage multiplier.

The VM on the transformer secondary side is driven by ac power generated by the LLC resonant inverter. A square wave voltage with a peak-to-peak value of V_{panel}/N is generated across the transformer secondary winding. The dc components are separated by the coupling capacitors C_1–C_4 connected to the secondary winding, and only the ac components pass through C_1–C_4. A dc voltage equivalent to the peak-to-peak value of the square wave voltage (i.e., V_{panel}/N) is outputted to each substring because each capacitor and diode pair (e.g., C_1, D_1, and D_2) comprises a voltage doubler [16].

Focusing only on the ac components yields the equivalent circuit, as shown in Fig. 7, in which all substrings as well as diode rectifiers are connected in parallel. The current automatically and preferentially flows toward shaded substrings having the lowest voltage in the panel, and the electrical characteristics of all substrings are automatically equalized [16].

IV. Experimental Results

A. Prototype

A 150-W prototype of the proposed converter that can supply 28 W for each shaded substring was built for four substrings connected in series, as shown in Fig. 8. Component values are listed in Table I. For the converter to operate with a duty cycle variation range of 0.2–0.8 at f_s = 100 kHz, f_r was designed to be 273 kHz, according to (4).

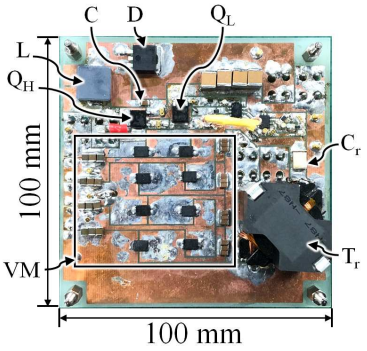

Fig. 8. 150-W prototype for four substrings.

TABLE I. Component Values

Component	Value
C_{in1}–C_{in4}	Ceramic Capacitor, 300 μF
D_1–D_8	Schottky Barrier Diode, V_f = 0.30 V
C_1–C_4	Ceramic Capacitor, 99 μF
C	Ceramic Capacitor, 33 μF
L	Inductor, 47 μH
D	Schottky Barrier Diode, V_f = 0.40 V
C_{out}	Ceramic Capacitor, 176 μF
C_r	Film Capacitor, 220 nF
Transformer	$N_1 : N_2$ = 12 : 3, L_{kg} = 1.54 μH, L_{mg} = 94.8 μH
Q_L–Q_H	FDD390N15A, $R_{DS(ON)}$ = 33.5 mΩ

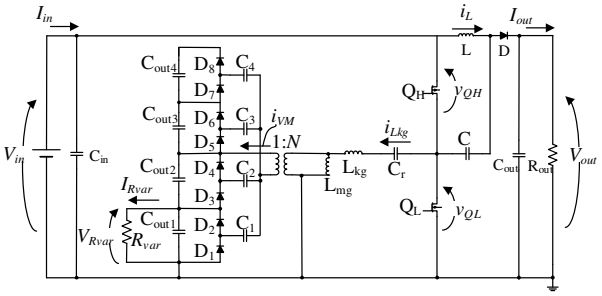

Fig. 9. Experimental setup for efficiency measurement.

B. Measured Waveforms and Power Conversion Efficiency

The experimental setup shown in Fig. 9 was employed to measure the operation waveforms and the power conversion efficiency. An external power supply was used as the input voltage V_{in}. A variable resistor R_{var} was connected to the output of the DPP converter to emulate the current flow paths under the condition where the PV1 is shaded. I_{Rvar} corresponds

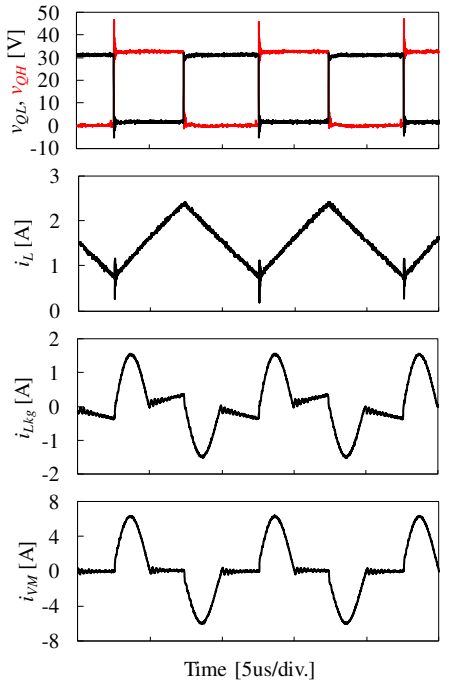

(a)

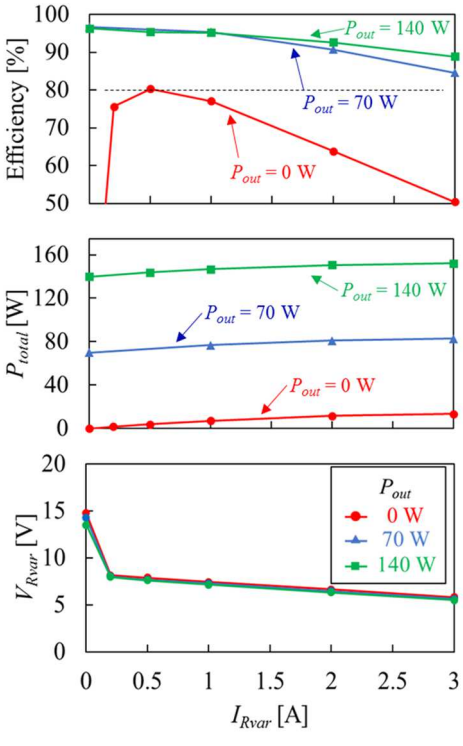

(b)

Fig. 10. (a) Measured waveforms and (b) power conversion efficiencies, total output powers, and output characteristics when PV1 is partially shaded.

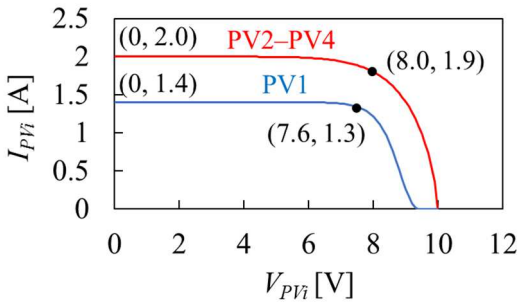

(a)

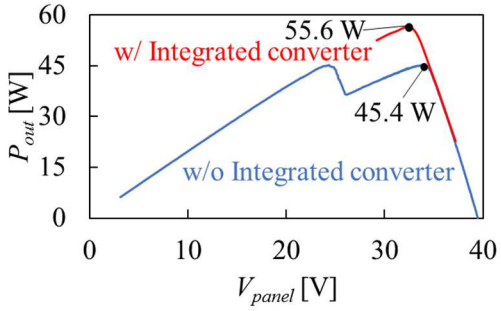

(b)

Fig. 11. Experimental equalization test: (a) Individual substring *I–V* characteristics, (b) *P–V* characteristics of the panel with/without integrated converter.

to the current difference between shaded and unshaded substrings. Power conversion efficiencies were measured with varying I_{Rvar} while the load power P_{out} was fixed to be 0, 70, or 140 W at V_{in} = 32 V and d = 0.5. In addition, P_{total}, a total output power of the DPP converter and the PWM step-up converter, and the output voltage of the DPP converter, V_{Rvar}, were also measured.

Measured waveforms at I_{Rvar} = 1.0 A and P_{out} = 70 W are shown in Fig. 10(a). The good agreement with the theoretical ones shown in Fig. 5 demonstrated the proper operation of the prototype.

The measured power conversion efficiencies, P_{total}, and V_{Rvar} are shown in Fig. 10(b). The case of P_{out} = 0 W was equivalent to the operation of the DPP converter alone and the output power of the step-up converter was zero. Therefore, the power conversion efficiency of the DPP converter alone was less than 80%. Similarly, the results at I_{Rvar} = 0 A indicated that the power conversion efficiency of the step-up converter alone was approximately 96%. These results suggested that the step-up converter was more efficient than the DPP converter because the efficiency decreased with the increase of I_{Rvar}. The most dominant loss factor in the DPP converter was considered to be conduction losses of the diodes because V_{Rvar} was mostly lower than 10 V. In addition, the increase in copper loss of the transformer was also considered to be a major loss factor. Since V_{Rvar} was independent on P_{out}, the output characteristics of the DPP converter was not affected by the step-up converter.

C. *Experimental Equalization Tests Emulating Partial Shading Condition*

An experimental equalization test using solar array simulators (E4361A, Keysight Technologies) was performed emulating the partial shading condition where PV1 was

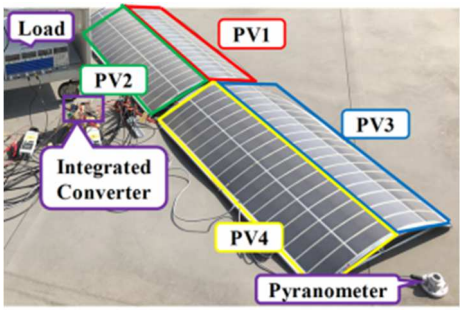

(a)

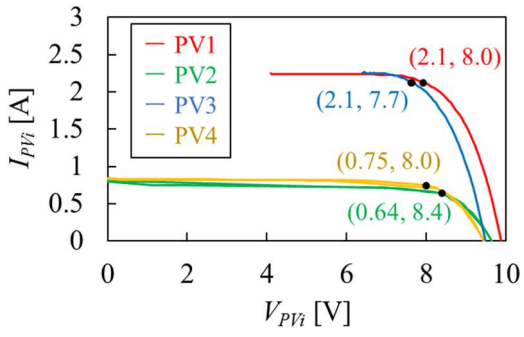

(b)

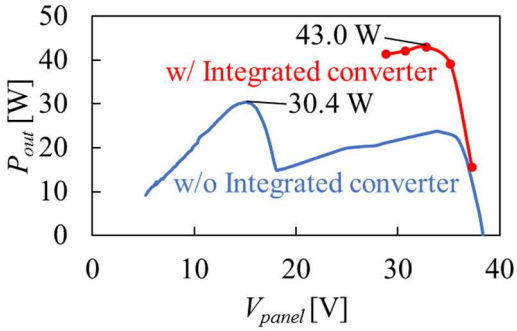

(c)

Fig. 12. Experimental equalization test: (a) Field test setup, (b) individual substring *I–V* characteristics, (c) *P–V* characteristics of the panel with/without integrated converter.

shaded. Individual substring characteristics used for the experiment are shown in Fig. 11(a). V_{out} was fixed at 48 V, and d was varied in the range of 0.3–0.7 to sweep PV panel characteristics. A bypass diode was also connected in parallel with each substring to compare panel characteristics with/without the integrated converter.

The measured *P–V* characteristics of the panel with/without the integrated converter are shown in Fig. 11(b). Without the integrated converter, two MPPs (global and local MPPs) on the *P–V* characteristics were observed, and the extractable maximum power was 45.4 W. With the integrated converter, conversely, the local MPP disappeared, and maximum power increased to as high as 55.6 W, corresponding to 22.5% improvement in power yield. The overall efficiency was approximately 99%—if all substrings could ideally operate at each MPP, the theoretical maximum power in the experimental condition was 55.7 W. The results demonstrated that the proposed converter could eliminate the partial shading issues.

D. Field Test Emulating Characteristic Mismatch Condition

The field testing was performed using two flexible panels, each consisting of two substrings, in Hitachi, Japan, at 15:00 on April 2019, as shown in Fig. 12(a). Assuming the PV panel mounted on a PHEVs' roof, the characteristic mismatch due to the curved surface was emulated. The solar irradiance was measured using a pyranometer, and the average solar irradiance was 495 W/m^2. Individual substring characteristics in the field testing are shown in Fig. 12(b). The theoretical maximum power was 44.6 W. V_{out} was fixed at 48 V, and d was varied in the range of 0.3–0.7.

The measured P–V characteristics of the panel with/without the integrated converter are shown in Fig. 12(c). The local MPP successfully disappeared, and the extractable maximum power increased from 30.4 W to 43.0 W by the proposed converter. This result corresponds to 41.4% improvement in power yield and the overall efficiency of approximately 96% (= 43.0 W / 44.6 W). Thus, the proposed converter precluded the negative influences under the mismatched condition in the field testing.

V. Conclusion

The PWM step-up converter integrating a DPP converter has been proposed for PV panels under partial shading in this paper. This converter can not only boost the panel voltage by PWM control but also automatically supply power to the shaded substrings without feedback control. The proposed converter achieves the reduction in the switch count and inductor miniaturization compared to a conventional power system using a separate DPP converter and traditional step-up converter. Therefore, the system simplification and circuit miniaturization are achieved by integrating two converters into a single unit.

Laboratory and field tests using the prototype were performed emulating partial shading and characteristic mismatch conditions. With the integrated converter, a local MPP disappeared, and the extractable maximum power improved by 22.5% and 41.4% in laboratory and field tests, respectively.

References

[1] T. Shimizu, M. Hirakata, T. Kamezawa, and H. Watanabe, "Generation control circuit for photovoltaic modules," *IEEE Trans. Power Electron*., vol. 16, no. 3, pp. 293–300, May 2001.

[2] K. A. Kim, P. S. Shenoy, and P. T. Krem, "Converter rating analysis for photovoltaic differential power processing systems," *IEEE Trans. Ind. Electron*., vol.30, no.4, pp.1987–1997, Apr. 2015.

[3] H. J. Bergveld, D. Büthker, C. Castello, T. Doorn, A. D. Jong, R. V. Otten, and K. D. Waal, "Module-level DC/DC conversion for photovoltaic systems: the delta-conversion concept," *IEEE Trans. Power. Electron*., vol. 28, no. 4, pp. 2005–2013, Apr. 2013.

[4] S. Qin, C.B. Barth, and R.C.N. Podgurski, "Enhancing microinverter energy capture with submodule differential power processing," *IEEE Trans. Power Electron*., vol. 31, no. 5, pp. 3575–3585, May 2016.

[5] F. Wang, T. Zhu, F. Zhuo, and H. Yi, "An improved submodule differential power processing-based PV system with flexible multi-MPPT control," *IEEE J. Emerging Selected Topics*, vol. 6, no. 1, pp. 94–102, Mar. 2018.

[6] A. Blumenfeld, A. Cervera, and M.M. Peretz, "Enhanced differential power processor for PV systems: resonant switched-capacitor gyrator converter with local MPPT," *IEEE J. Emerging Selected Topics in Power Electron*., vol. 2, no. 4, pp. 883–892, Dec. 2014.

[7] Z. Qiu and K. Sun, "A photovoltaic generation system based on wide voltage-gain DC-DC converter and differential power processors for DC microgrids," *Chinese J. Electrical Engineering*, vol. 3, no. 1, pp. 84–95, Jun. 2017.

[8] A. H. Chang, A. T. Avestruz, and S. B. Leeb, "Capacitor-less photovoltaic cell-level power balancing using diffusion charge redistribution," *IEEE Trans. Power. Electron*., vol. 30, no. 2, pp. 537–546, Feb. 2015.

[9] M. Uno, Y. Saito, M. Yamamoto, and S. Urabe, "PWM switched capacitor-based cell-level power balancing converter utilizing diffusion capacitance of photovoltaic cells," *IEEE Trans. Power Electron*., to be published.

[10] M. Uno, M. Yamamoto, H. Sato, and S. Oyama, "Modularized differential power processing architecture based on switched capacitor converter to virtually unify mismatched photovoltaic panel characteristics," *IEEE Trans. Power Electron*., to be published.

[11] M. Gokdaga, M. Akbabab, and O. Gulbudakc, "Switched-capacitor converter for PV modules under partial shading and mismatch conditions," *Solar Energy*, vol. 170, pp. 723–731, Aug. 2018.

[12] C. Olalla, D. Clement, M. Rodríguez, and D. Makisimović, "Architectures and control of submodule integrated dc-dc converters for photovoltaic applications," *IEEE Trans. Power Electron*., vol. 28, no. 6, pp. 2980–2997, Jun. 2013.

[13] R. Bell and R.C.N.P. Podgurski, "Decoupled and distributed maximum power point tracking of series-connected photovoltaic submodules using differential power processing," *IEEE J. Emerging Selected Topics in Power Electron*., vol. 3, no. 4, pp. 881–891, Dec. 2015.

[14] Y.T. Jeon, H. Lee, K.A. Kim, and J.H. Park, "Least power point tracking method for photovoltaic differential power processing systems," *IEEE Trans. Power Electron*., vol. 32, no. 3, pp. 1941–1951, Mar. 2017.

[15] Y.T. Jeon and J.H. Park, "Unit-minimum least power point tracking for the optimization of photovoltaic differential power processing systems," *IEEE Trans. Power Electron*., vol. 34, no. 1, pp. 311–324, Jan. 2019.

[16] M. Uno and A. Kukita, "Two-switch voltage equalizer using an LLC resonant inverter and voltage multiplier for partially-shaded series-connected photovoltaic modules," *IEEE Trans. Ind. Appl*., Vol. 51, No. 2, pp. 1587–1601, Mar/Apr. 2015.

[17] M. Uno and A. Kukita, "PWM converter integrating switched capacitor converter and series-resonant voltage multiplier as equalizers for photovoltaic modules and series-connected energy storage cells for exploration rovers," *IEEE Trans. Power Electron*., vol. 32, no. 11, pp. 8500–8513, Nov. 2017.

[18] M. Uno and A. Kukita, "Single-switch voltage equalizer using multi-stacked buck-boost converters for partially-shaded photovoltaic modules," *IEEE Trans. Power Electron*., vol. 30, no. 6, pp. 3091–3105, Jun. 2015.

[19] M. Uno and A. Kukita, "Current sensorless equalization strategy for a single-switch voltage equalizer using multistacked buck–boost converters for photovoltaic modules under partial shading," *IEEE Trans. Ind. Appl*., vol. 53, no. 1, pp. 420–429, Jan./Feb. 2017.

[20] M. Uno and A. Kukita, "Single-switch single-magnetic PWM converter integrating voltage equalizer for partially-shaded photovoltaic modules in standalone applications," *IEEE Trans. Power Electron*., vol. 33, no. 2, pp. 1259–1270, Feb. 2018.

[21] M. Uno and T. Shinohara, "Variable switching frequency modulation scheme for PWM converter integrating series-resonant voltage multiplier-based voltage equalizer for photovoltaic strings under partial shading," *IEEJ Trans. Electrical Electronics Engineering*., vol. 14, no. 3, pp. 467–474, Mar. 2019.

[22] M. Uno and T. Shinohara, "Module-integrated converter based on cascaded quasi-Z-source inverter with differential power processing capability for photovoltaic panels under partial shading," *IEEE Trans. Power Electron*., to be published.

[23] M. Uno, T. Shinohara, Y. Saito, and A. Kukita, "Review, comparison, and proposal for PWM converters integrating differential power processing converter for small exploration rovers," *Energies*, pp. 1–19, May 2019.